*Indonesian Journal of Aerospace Vol. 24 No. 1 June 2026 : pp 17–34 (Wuwung et al.)*
DOI: 10.55981/ijoa.2026.13060
https://ejournal.brin.go.id/ijoa/

# Numerical Simulation Analysis of Injector Placement for Optimum Fuel/Air Mixture in Mini Turbojet Combustion Chamber with 200N Static Thrust

**Vicky Wuwung*, Aura Saum Mulyadi, Reina Fadjrin Nurul Anissa, Wenty Anggraeni, Radi Suradi Kartanegara**

Jurusan Teknik Mesin, Politeknik Negeri Bandung, Bandung 40012
*e-mail: vicky.wuwung@polban.ac.id

Received: 30/07/25 Revised: 07/02/2026 Accepted: 27/02/2026 Published: 26/10/2026

## Abstract

A turbojet engine is a simple jet engine. Small turbojets utilize gas turbines to generate hot gas, which is then directed to the nozzle at a higher temperature. The development of mini turbojets at Polban began with the creation of combustion chamber geometry and the determination of the number and location of injectors for efficient combustion. The process of mixing fuel and air, as well as combustion within the combustion chamber of the mini turbojet with a thrust of 200 N, was analysed numerically in this study. This study employed a Computational Fluid Dynamics (CFD) approach based on the k-epsilon turbulence model to optimize the design of the annular combustion chamber with 154 air holes and 11 fuel injectors. Additionally, simulations of mixing and combustion within the combustion chamber were conducted as a form of validation. Based on the simulation results, changes in injector position caused an increase in the recirculation zone, which initially involved one injector out of eight, to eight out of eleven injectors, helping to maintain combustion stability and achieve thermal efficiency of 78.29%. With a temperature ratio (TR) of 3.064 and a pressure ratio (PR) of 0.39, the ideal airflow distribution produces toroidal vortices in the primary and secondary zones. With recommendations for further optimization to enhance performance under various operating conditions, these findings provide useful guidance for the development of a more stable and efficient mini-turbojet combustion chamber.

***Keywords***: Mini turbojet combustion chamber, numerical simulation, combustion efficiency, injector optimization, steady flow.

## Nomenclature

| | | |
|---|---|---|
| $a$ | = | Air mass flow rate, (kg/s) |
| $\dot{m}_p$ | = | Primary zone air mass flow rate, (kg/s) |
| $\dot{m}_s$ | = | Secondary zone air mass flow rate, (kg/s) |
| $\dot{m}_d$ | = | Dilution zone air mass flow rate, (kg/s) |
| $f$ | = | Fuel mass flow rate, kg/s |
| $T_{02}$ | = | Total temperature at combustor inlet, (K) |
| $T_{03}$ | = | Total temperature at combustor outlet, (K) |
| $P_{02}$ | = | Total pressure at combustor inlet, (Pa) |
| $P_{03}$ | = | Total pressure at combustor outlet, (Pa) |
| $\Delta p_0$ | = | Total pressure losses between inlet and outlet combustion chamber, (%) |
| $\rho_{02}$ | = | Total density at combustor inlet (kg/m$^3$) |
| U | = | Annular Airflow Inlet velocity (m/s) |
| $C_3$ | = | Combustion Chamber Absolute Outlet Velocity (m/s) |



e-ISSN 2597-7873 (online) | © 2026 The Author(s). Published by BRIN Publishing.
This is an open access article under the CC BY-SA license(https://creativecommons.org/licenses/by-sa/4.0/)
IJOA accredited as Sinta 2 Journal (https://sinta.kemdikbud.go.id/journals/profile/3362)

| | | |
|---|---|---|
| $\rho$ | = | Density, (kg/m³) |
| $\rho_f$ | = | Fuel density (kg/m³) |
| $\rho_{cf}$ | = | Crossflow air density (kg/m³) |
| $C_d$ | = | Discharge coefficient of injector |
| $Uf$ | = | Fuel velocity at injector outlet, (m/s) |
| $Ucf$ | = | Effective fuel velocity after compression, (m/s) |
| D | = | Injector diameter, (mm) |
| z, x | = | Penetration distance from outlet injector in combustion chamber, (mm) |
| LHV | = | Lower Heating Value of Propane, (kJ/kg) |
| TR | = | Temperature Ratio |
| PR | = | Pressure Ratio |
| $\varepsilon\varepsilon$, k | = | Turbulence dissipation rate and kinetic energy |
| $Y^+$ | = | Dimensionless wall distance |
| CFL | = | Courant–Friedrichs–Lewy number (for solver stability) |
| CFD | = | Computational Fluid Dynamics |
| DRO | = | Design Requirement and Objective |
| LES | = | Large Eddy Simulation |
| RANS | = | Reynolds-Averaged Navier–Stokes |
| FAR | = | Fuel–Air Ratio |
| H, V | = | Injector displacement (mm) |
| $C_3H_8$ | = | Propane |

## 1. Introduction

Mini turbojet engines are increasingly being developed for applications in unmanned aerial vehicles (UAVs), experimental propulsion systems, and educational platforms due to their compact size, relatively simple system configuration, and ease of integration. However, efficient fuel–air mixing and stable combustion are still difficult to achieve in mini combustion chambers. This challenge is caused by the residence time available for the airflow to remain inside the combustion chamber, the high axial flow velocity, and the geometric constraints of the combustion chamber. Together, these factors can reduce mixing quality and make flame stabilization more difficult. In the combustion chamber, the compressed air will be distributed to ptimary zone, secondary zone and dilution zone, where the primary zone plays an important role to maintaining flame stability through the formation of a recirculation zone. In the combustion chamber, compressed air is distributed into the primary, secondary, and dilution zones, where the primary zone plays an important role in maintaining flame stability through the formation of a recirculation zone. (Saravanamuttoo et al., 2017).

The recirculation zone is a low velocity reverse flow region formed by the interaction of swirling flow and flow separation. In this zone, high temperature combustion products circulate back to the primary zone, helping the incoming air mix with the fuel, increasing residence time inside the combustion chamber, and improving flame stability. Previous studies showed that flame stability improves when a strong recirculation zone is formed and combustion efficiency (Fuchs dkk., 2019).. However, in mini turbojet combustion chambers, the formation of the recirculation zone is highly influenced by the number and placement of injectors, as well as the airflow distribution, due to the smaller combustor size and limited geometric dimensions.

Santosa (2022) investigated a 200 N thrust mini turbojet combustion chamber. However, the study did not provide an in-depth analysis of injector placement and mainly focused on the airflow characteristics inside the combustion chamber. The research was conducted using analytical methods and Computational Fluid Dynamics (CFD) simulations. The study examined the formation of the recirculation zone in the primary zone based on airflow characteristics.

This result differs from the findings reported by Capata and Achille (2018). They found that improper injector placement may cause the fuel jets to hit the combustion chamber liner wall. As a result, the fuel–air mixing becomes less uniform, while the vortical structures near the wall are weakened. This condition can further increase the local temperature around the wall. It can also impose a high thermal load on the liner and accelerate material degradation. Improper injector placement may also affect the mixing uniformity and increase pressure losses in the combustion chamber.

Syarifudin (2022) investigated a mini turbojet engine with a thrust range of 100–200 N using different injector configurations, with the number of injectors varying from four to eight. The study mainly discussed overall engine performance, including exhaust gas temperature and CO emissions. However, the flow behavior inside the combustion chamber was not examined in detail. The formation of the primary recirculation zone and its strength were also given limited attention, although both are important for maintaining flame stability. Therefore, the effect of injector placement on vortex formation near the liner wall and the development of the primary recirculation zone is still not fully understood.

Although many studies have been carried out on micro-turbojet engines and small-scale combustion chambers, the effect of injector configuration on the internal flow field has received less attention. Previous studies have mainly focused on engine performance, thermodynamic validation, and general combustion chamber geometry (Badami et al., 2013; Wessley, 2019). The flow structure inside the combustion chamber, particularly the formation of recirculation zones and vortices, has therefore not been fully investigated.

The relationship between injector diameter, the number of injectors, and their placement with the formation and strength of the primary recirculation zone also needs further investigation (Santoso, 2022; Syarifudin, 2022). Vortices formed near the liner wall may be influenced by the use of small-diameter fuel injectors and can affect the uniformity of fuel–air mixing. This aspect has received limited attention, especially in compact turbojet engines operating at low fuel mass flow rates. Most previous studies have focused on combustion temperature and efficiency, while the mixing process inside the combustor has generally received less discussion (Habibi et al., 2019; Kotze, 2018). As a result, the flow mechanisms that contribute to flame stabilization are not yet completely clear. The effect of injector momentum on vortex formation near the liner wall and its relationship with the stability of the primary recirculation zone also remains an area that requires further study.

In this study, the mini turbojet engine operates at a rotational speed of 55,000 rpm, which is relatively low compared with typical turbojet operating conditions. At this rotational speed, the required fuel mass flow rate is relatively low, so a small injector diameter is used to maintain an air-to-fuel ratio of 1:15. With a smaller injector diameter, even a small change in injector position can influence the flow pattern inside the combustion chamber. Changes in the direction or momentum of the fuel jet may affect vortex formation, the flow behavior near the liner wall, and fuel–air mixing in the primary zone.

Figure 1-1 shows the airflow distribution within the liner, together with the flow entering the combustion chamber and forming the recirculation zone. Unlike the previous studies discussed above, this study considers the preliminary design of a fuel injection system for

a 200 N mini-turbojet combustion chamber in which the injector configuration has not yet been specifically defined.

This study aims to determine the fuel injector configuration, including the number, diameter, and placement of the injectors, using analytical calculations followed by verification through Computational Fluid Dynamics (CFD) simulations. The selected configuration is expected to provide a fuel–air mixing ratio of 1:15, establish a stable primary recirculation zone, and minimize vortex formation near the combustor liner wall. The mixing stage focuses on the flow behavior inside the combustor, particularly the velocity and pressure distributions. Since propane is supplied in the gaseous phase, temperature effects are not considered during this stage. During the combustion stage, however, temperature distribution becomes an important parameter because it is closely related to ignition and flame stability. Through the combined use of analytical calculations and CFD simulations, this study aims to develop an injector configuration that enhances mixing uniformity, stabilizes combustion, and minimizes local thermal loading on the combustion chamber liner.

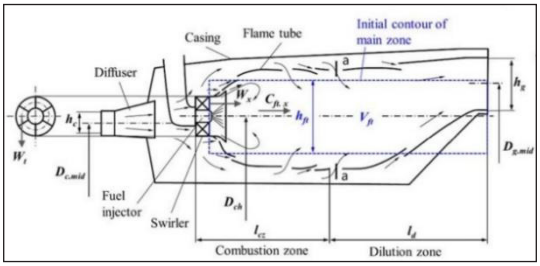



**Figure 1-1:** Liner Airflow Distribution

## 2. Methodology

The small-scale turbojet engine was developed based on the Design Requirement Objective (DRO) and thermodynamic calculations. The combustion chamber has an annular configuration, and its design was based on the Lefebvre method. The injector arrangement was first determined from analytical calculations and was then assessed through Computational Fluid Dynamics (CFD) simulations. The purpose of this analysis was to obtain better fuel–air mixing while still maintaining stable combustion.

For the CFD analysis, the standard k–ε RANS turbulence model was chosen. This model is commonly applied in engineering flow simulations and provides relatively stable numerical results. A one-step global reaction mechanism was also used to reduce the computational requirements of the simulation. With this approach, the simulation can be used to examine fuel–air mixing, temperature distribution, and the overall combustion performance. However, the model is not intended to provide a detailed prediction of emissions such as CO and NOx.

The combustion chamber was first evaluated through analytical calculations before proceeding to the CFD simulation. The Lefebvre method was applied to estimate the chamber geometry, airflow distribution in the different liner zones, characteristics of the recirculation zone, and the allowable pressure drop for the 200 N mini-turbojet combustion chamber. The analytical results were subsequently compared with the CFD results.

Rather than focusing only on the agreement between analytical and numerical results, this study examines how the injector position affects the flow inside the combustion chamber. Eleven injector configurations were considered under steady-state conditions. The different configurations were used to observe changes in the recirculation zone and combustion behavior

associated with the injector position. The complete procedure followed in this study is presented in Figure 2-1.

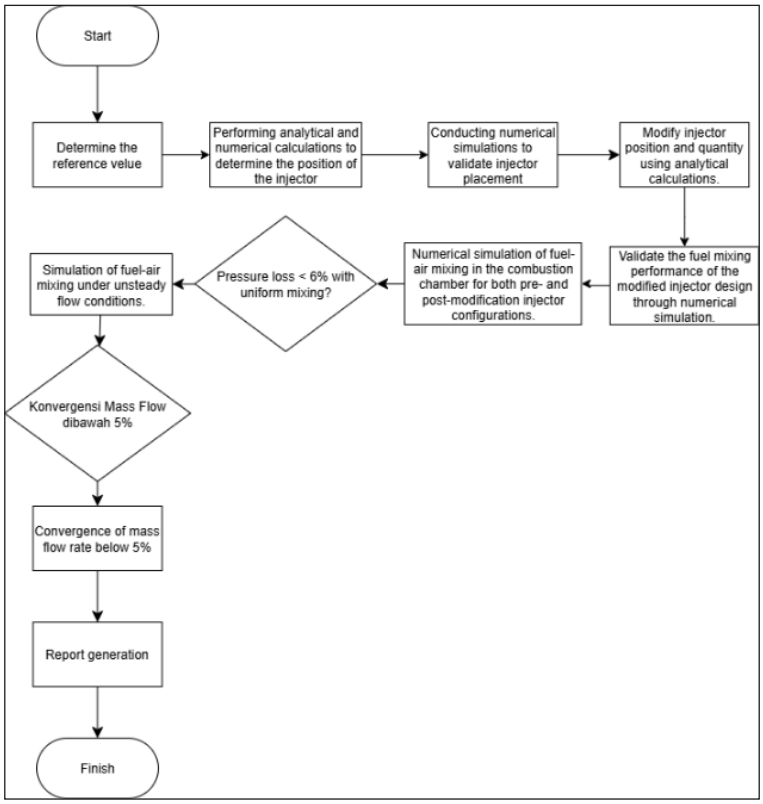



**Figure 2-1:** Injector Design and Optimization Methodology

The study examined an annular combustion chamber designed for a 200 N-class mini turbojet engine, featuring a 113.64 mm length and 148 mm outlet diameter (Figure 2-2). This combustion chamber has 140 air holes divided into three zones: the primary zone with a hole diameter of 2.153 mm, the secondary zone with 2.503 mm, and the dilution zone with 5.005 mm. Eleven 1-mm-diameter fuel injectors are arranged in a circular pattern around the primary zone to aid in the formation of the vortices and toroidal circulation necessary for maintaining flame stability. Airflow distribution is controlled by directing 20% of the air to the primary zone, 20% to the secondary zone, and 60% to the dilution zone. Based on the results of analytical calculations and CFD simulations, this design produces a pressure drop ranging from 4% to 10.86% and is capable of achieving good fuel–air mixing and combustion in the mini-turbojet combustion chamber.

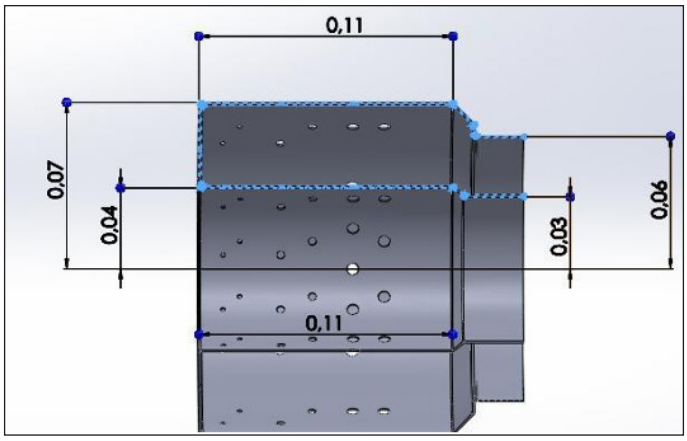



**Figure 2-2:** Geometry Combustion Chamber (Santoso, 2022)

The design of a small turbojet engine with a target thrust of 200 N using propane fuel is based on simulations of the compressor's mass flow rate and total outlet temperature. Throughout the design process, mixing simulation, and combustion, these parameters—which are shown in Tables 2-1 and 2-2 are used consistently.

**Table 2-1:** Initial Design Parameters

| Symbol | Name | Value |
|---|---|---|
| $\dot{m}_a$ | Air mass flow | 0,55 Kg/s |
| $T_{02}$ | Total of combustor temperature inlet | 390,514 K |
| $P_{02}$ | Total of combustor pressure inlet | 243180 Pa |
| $FAR$ | Fuel air ratio at primary zone | 0,0664 |
| $T_{03}$ | Total of combustor temperature outlet | 997,51 K |
| $P_{03}$ | Total of combustor pressure outlet | 233452 Pa |
| $C_3$ | Combustor outlet Absolute Velocity | 99.79 m/s |
| $\rho\rho_{02}$ | Total density combustor inlet | 1,6 Kg/m3 |

**Table 2-2:** Design Reference Output

| Parameter | Value | Unit |
|---|---|---|
| Thrust | 200 | N |
| Intake air pressure | 101325 | Pa |
| Intake air temperature | 288.15 | K |
| Air mass flow rate | 0.55 | Kg/s |
| Fuel mass flow rate | 0.007425 | Kg/s |
| Fuel type | Propana ($C_3H_8$) | - |
| Initial injector diameter | 1 | mm |
| Number of initial injectors | 9 | injectors |
| Combustion chamber type | Annular | - |

Temperature ratio is the ratio of the initial temperature to the final temperature. For example, the temperature ratio in the combustion chamber is calculated using the equation $TR = \frac{T_{03}}{T_{02}}$. The goal is to understand the change in thermal energy (H.I.H. Saravanamuttoo, H. Cohen & A.C. Nix, 2017).

Pressure ratio is the ratio of the final pressure at the outlet to the initial pressure at the combustion chamber inlet. For example, the temperature ratio in the combustion chamber is calculated using the equation $PR = \frac{P_{03}}{P_{02}}$ . The goal is to understand the change in heat energy (H.I.H. Saravanamuttoo, H. Cohen & A.C. Nix, 2017).

Fuel and air are burned in the combustion chamber to produce heat. All of the fuel completely reacts with oxygen when the air to fuel ratio is stoichiometric, leaving no residue behind. Combustion is most effective at this point. For instance, propane has a stoichiometric air-fuel ratio of 15.6:1, which means that 1 kilogram of propane requires 15.6 kilograms of air to burn. The mixture is referred to as rich if there is less air than this. A mixture is referred to as lean if it contains more air. Active stoichiometry adjustment can increase combustion stability, particularly in the primary combustion zone. By postponing flame blowout and flashback, this increases the engine's operating limits (Chmielewski et al., 2016).

The injector was analytically designed to disperse fuel uniformly in the annular combustion chamber's primary zone based on Bernoulli and the laws of continuity. A circulation zone

is formed in each spray due to the symmetrical placement of nine 1 mm diameter injectors around the combustion chamber. Analytical calculations can be seen in equation 2-1 (Z. P. Tan, 2017), where this equation and varying the injector diameter and fuel velocity will yield the penetration range ratio. However, initial simulations indicate that a stable circulation zone is formed by only one spray.

$$\frac{x}{d_f} = \sqrt{\frac{z}{d_f}\left(\frac{\pi}{C_d}\right)\left(\frac{\rho_f U_f^2}{\rho_{cf} U_{cf}^2}\right)} \tag{2-1}$$

The CFD simulation setup begins with CAD-designed geometry (Parasolid format) of the injectors and annular combustion chamber, including gas outlet duct, injector nozzle, and air intake duct. This geometry is imported into Numeca software for meshing and simulation. An unstructured hexahedral mesh was used to represent the flow inside the combustion chamber. In the regions close to the walls, the mesh was generated with a Y+ value of approximately 5. Air and propane ($C_3H_8$) were included as the main species in the multi-species model. The Extended Wall Function k–ε model was adopted to describe the turbulent flow in the combustion chamber. The first simulation was performed without combustion reactions under steady-state conditions. At this stage, the flow field and fuel–air mixing inside the chamber were examined.

The simulation results were then used as a reference for evaluating the injector positions and their effect on the circulation distribution. After the mixing analysis, the combustion simulation was carried out using the same geometry and injector configuration. The walls of the combustion chamber were assumed to be adiabatic during the combustion simulation.

In accordance with the journal (Santoso et al., 2023), this analysis employs a global single-step reaction model with reference conditions of pressure 243.180 Pa and temperature 390.51 K in addition to the RANS k-ε Yang-Shih turbulence model enhanced with extended wall functions and Y+. In order to assess efficiency, a density-based solver with an improved CFL number speeds up convergence. During the combustion stage, temperature distribution, pressure drop, circulation patterns, and combustion efficiency were compared using the same boundary conditions as in the mixing stage. This comparison was used to assess the combustion chamber performance under operating conditions close to the actual conditions.

## 3. Result and Analysis

Computational Fluid Dynamics (CFD) was used to study the fuel–air mixing and combustion inside the mini-turbojet combustor. The simulation was carried out in two stages. The first stage considered the flow without combustion under steady-state conditions. The flow pattern in the combustor was examined at this stage, with particular attention to the primary recirculation zone and the vortices formed near the liner wall. The combustion calculation was carried out in the second stage. The temperature field and combustion behavior were then evaluated. The parameters considered in both stages included the fuel–air mixing ratio, pressure drop, and velocity distribution, while temperature distribution and combustion efficiency were evaluated during the combustion stage.

Several injector configurations were considered by changing the injector diameter, number, and position. The changes in these parameters affected the flow inside the combustor and, consequently, the combustion behavior. The velocity and pressure fields were examined to assess the fuel–air mixing. The flow near the liner wall was also observed, especially in areas

where the recirculation was weak or vortices were present. During the combustion stage, the temperature field was examined to evaluate the flame behavior, heat release, and thermal load on the liner.Combustion efficiency was also calculated to evaluate the performance of each injector configuration in producing a stable combustion process.

The selected injector arrangement produced a more uniform fuel–air mixture and a stronger primary recirculation zone more uniform fuel–air mixing and strengthening the primary recirculation zone. In addition, vortex formation near the liner wall can be reduced, resulting in a more stable combustion process in the mini-turbojet combustion chamber.

### 3.1 Injector Design and Grid Convergence Study Results

Injector design variations with diameters ranging from 0.1 to 5 mm were calculated using Equation (2-1), with the results presented in Table 3-1 and Figure 3-1. Based on the analysis, an injector diameter of 1 mm producing a fuel flow deflection angle of 89.4° (Z/x) was identified as optimal. This large deflection angle is caused by the high velocity of the primary annular airflow, which promotes the formation of a recirculation zone in the primary combustion region.

**Table 3-1:** Calculation of Injector Diameter Variation

| D | Cd | $\rho_f$ | $U_f$ | $\rho_{cf}$ | $U_{cf}$ | $\frac{x}{\sqrt{Z}}$ | z | x |
|---|---|---|---|---|---|---|---|---|
| 5 | 0,8 | 493 | 0,06976654 | 1,4 | 67,3 | 0,002725 | 0,01123892 | 0.000289 |
| 4 | 0,8 | 493 | 0.10901022 | 1,4 | 67,3 | 0.003809 | 0.01123892 | 0.000404 |
| 3 | 0,8 | 493 | 0.19379595 | 1,4 | 67,3 | 0.005864 | 0.01123892 | 0.000622 |
| 2 | 0,8 | 493 | 0.43604088 | 1,4 | 67,3 | 0.010772 | 0.01123892 | 0.001142 |
| 1 | 0,8 | 493 | 1.74416351 | 1,4 | 67,3 | 0.030469 | 0.01123892 | 0.00323 |
| 0,9 | 0,8 | 493 | 2.15328829 | 1,4 | 67,3 | 0.035685 | 0.01123892 | 0.003783 |
| 0,8 | 0,8 | 493 | 2.72525549 | 1,4 | 67,3 | 0.042581 | 0.01123892 | 0.004514 |
| 0,7 | 0,8 | 493 | 3.55951737 | 1,4 | 67,3 | 0.052024 | 0.01123892 | 0.005515 |
| 0,6 | 0,8 | 493 | 4.84489864 | 1,4 | 67,3 | 0.065558 | 0.01123892 | 0.00695 |
| 0,5 | 0,8 | 493 | 6.97665405 | 1,4 | 67,3 | 0.086178 | 0.01123892 | 0.009136 |
| 0,4 | 0,8 | 493 | 10.901022 | 1,4 | 67,3 | 0.120437 | 0.01123892 | 0.120437 |
| 0,3 | 0,8 | 493 | 19.3795946 | 1,4 | 67,3 | 0.185426 | 0.01123892 | 0.019658 |
| 0,2 | 0,8 | 493 | 43.6040878 | 1,4 | 67,3 | 0.340648 | 0.01123892 | 0.036113 |
| 0,1 | 0,8 | 493 | 174.416351 | 1,4 | 67,3 | 0.963499 | 0.01123892 | 0.102144 |

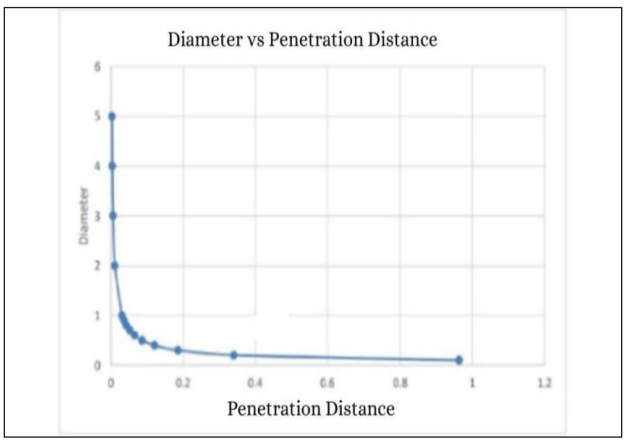



**Figure 3-1:** Diameter vs. Penetration Distance Curve

**Table 3-2:** Study Grid

| No | Grid Type | Number of Cells |
|---|---|---|
| *1* | Grid 0 | 11.391.101 |
| *2* | Grid 1 | 14.269.832 |
| 3 | Grid 2 | 16.640.469 |
| *4* | Grid 3 | 18.930.790 |
| *5* | Grid 4 | 21.485.064 |

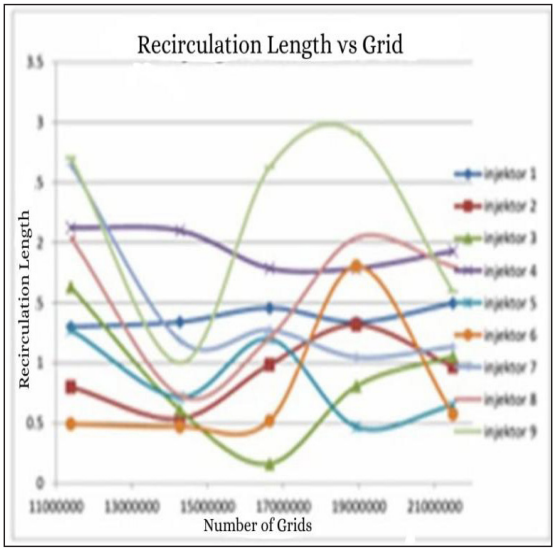



**Figure 3-2:** Size Curve x Vs Number of Grids

The third curve above (Figure 3-2) shows the estimated point of convergence. Data from each injector can be obtained at five different grids. Grid 3 also seems to be highly convergent, even though grid 2 does as well. Grid 2 is deemed optimal with an error of less than 1%, according to the grid convergence test (Table 3-2). Both options lead to the conclusion that grid 2, or a grid with few cells that has converged, is the best grid. The convergence criterion is one element affecting the simulation's outcomes. This is confirmed by looking at the continuity equation with a difference between the incoming and outgoing fluid in the domain of less than 1%, as well as flow convergence with an error level or rate of less than $10^{-3}$. The visualization of the data in Table 3-2 can be seen in Figure 3-3, where the grid has a total of 16.6 million cells.

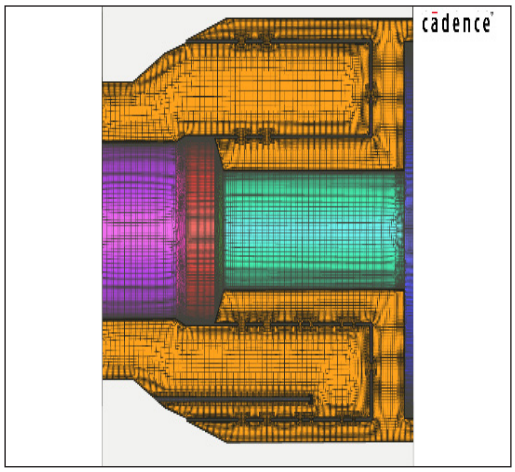



**Figure 3-3:** Combustion Chamber Hexahedral Unstructured Grid

### 3.2 Injector Placement Cold Flow Simulation Result (Recirculation Zone, Fuel/Air Mixing, and Near Wall Vortex).

The injector placement locations based on simulation data are displayed in Figures 3-4. The figure illustrates the flow field inside a mixing chamber with a side injector. The contour colours indicate the velocity distribution and the streamlines show the flow direction. H and V represent the chamber length and height, while X and Z denote the horizontal and vertical coordinates. The circular region in the figure shows the recirculation zone. Vortices can be observed in this region, along with stronger fluid mixing. Once the injector position was determined from the H and V distances, the x, z, and Ucf data were taken from this zone. The data were then used to evaluate the flow around the combustion chamber liner.

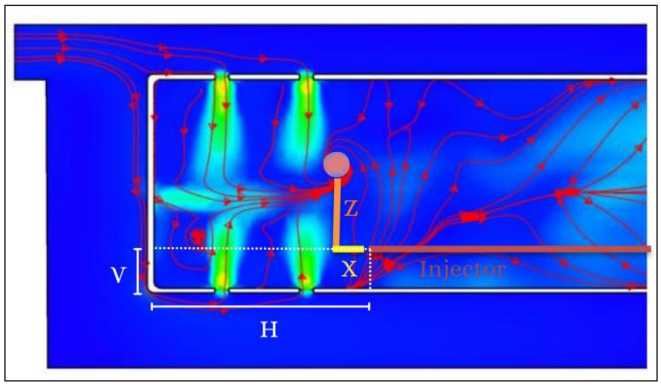



**Figure 3-4:** Placement of the "H, V, x, z Distance" Injector

Table 3-3 compares the original and modified injector configurations. In the initial configuration, most of the injectors did not generate a strong recirculation zone in the primary combustion region. From the velocity contours, the flow can be seen to remain mainly in the axial direction. The fuel jets either stayed close to the liner wall or moved downstream without producing a stable vortex. As a result, the fuel–air mixing was less effective and the residence time of the mixture inside the combustion chamber was reduced. These conditions made it more difficult to maintain stable combustion.

Among the initial configurations, injector 1 was the only one that produced a relatively well-developed recirculation zone. The other configurations either produced small vortices in localized areas or did not show a clear recirculation zone. This behavior was observed at injector angles of 120°, 160°, 200°, and 240°. At these positions, the flow was still dominated by weak vortices, and the interaction between the fuel jet and the annular airflow was limited. The weak recirculation indicates that the fuel jet did not transfer sufficient momentum to the main airflow. This makes flame stabilization more difficult and also leads to poor mixing at a fuel–air ratio of 1:118, which may contribute to combustion instability.

To improve this condition, the injectors were repositioned using a horizontal distance (H) of 22.6 mm and a vertical distance (V) of 7.49 mm. The number and diameter of the injectors were kept unchanged. With this new position, the fuel spray was placed closer to the primary recirculation zone. This allowed greater interaction between the fuel jet and the recirculating airflow, which was expected to improve the mixing process. Such momentum matching between the fuel jet and surrounding flow enhances vortex formation and stabilizes toroidal recirculation zones, thereby increasing residence time and mixing efficiency (Saravanamuttoo et al., 2017; Fuchs et al., 2019). As a result, the modified injector configuration produces a significantly improved flow structure across most angular positions. As illustrated in the left column of Table 3-3, seven out of eleven injectors ( injector no. 1, 3, 4, 6, 7, 10, and 11) that is associated

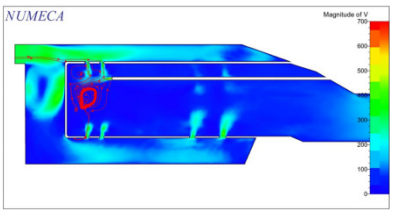
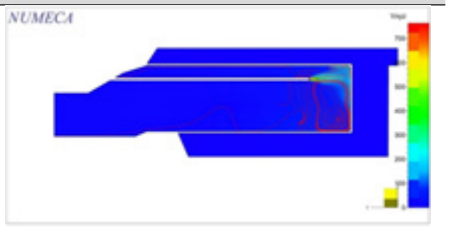
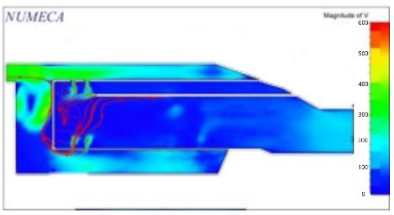
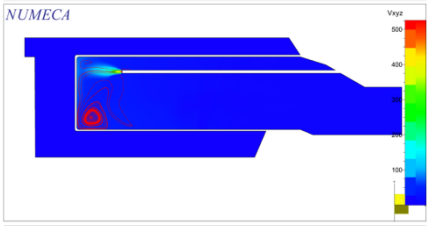
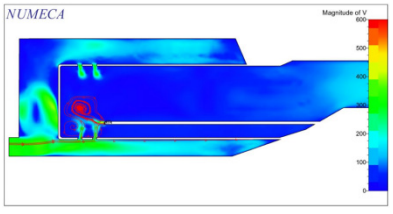
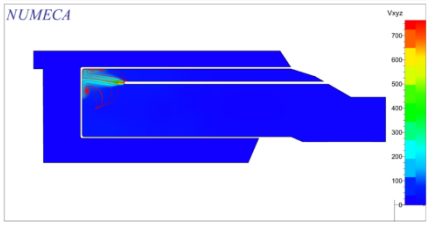
with cutting plane angle 32°, 98°, 130°, 196°, 229°, 327°, and 360°, generate a distinct and well-developed recirculation zone characterized by closed streamlines and localized low-velocity regions near the primary zone.

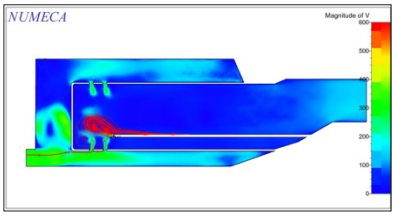
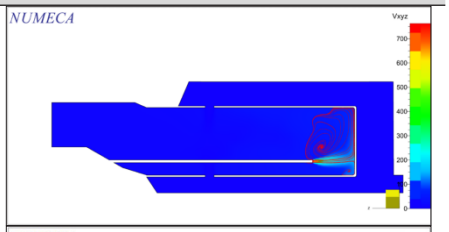
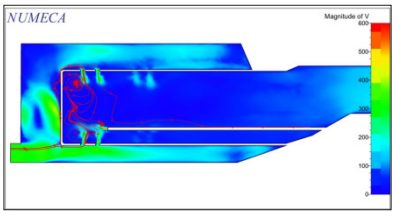
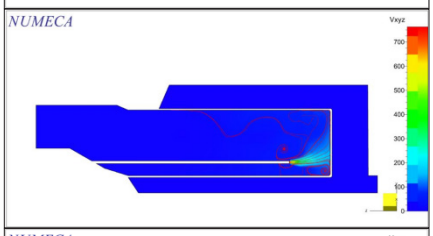
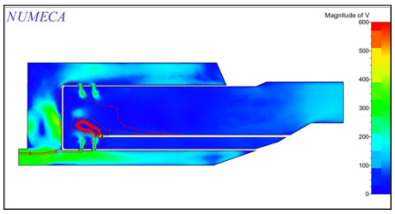
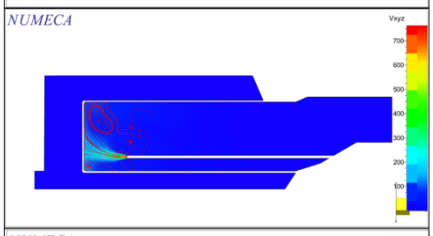
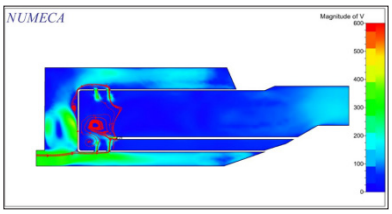
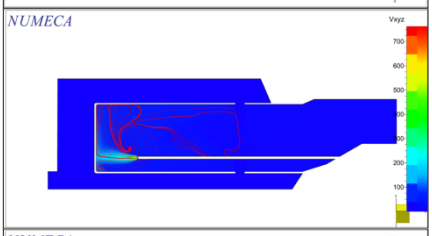
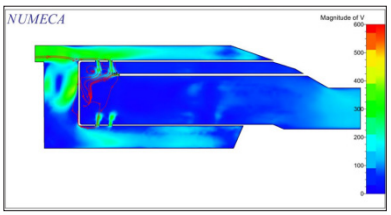
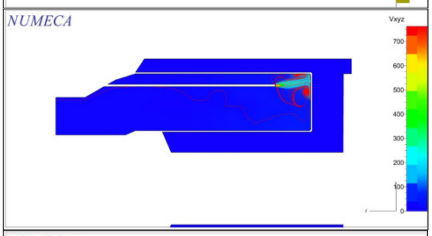
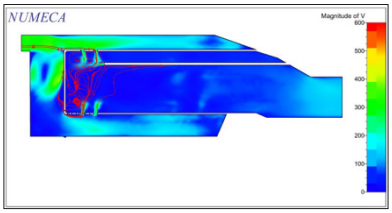
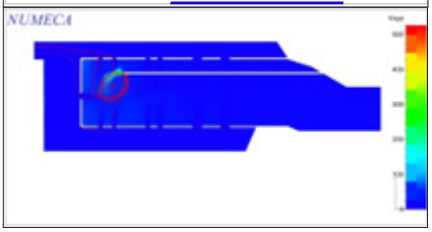
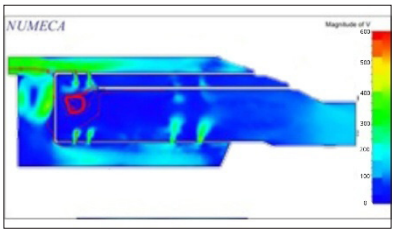
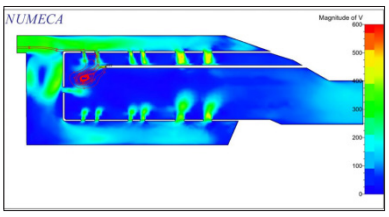
This optimized configuration produces an average circulation size in 10.25 mm, distance of x = 4.92 mm, and z = 5.52 mm from the injector outlet, indicating improved fuel retention and mixing within the high-temperature region, consistent with previous numerical findings (Santoso, 2022; Topal et al., 2015). The formation of these vortical structures indicates stronger interaction between the fuel jets and the surrounding axial and annular airflow. The redistribution of injector angular positions enhances radial jet penetration, reduces wall-attached flow behaviour, and promotes more symmetric mixing within the combustor liner.

Furthermore, the modified injector layout induces a stronger swirling motion in the primary zone, as evidenced by the expanded recirculation regions and intensified shear layers visible in the velocity magnitude contours. This swirling effect increases turbulence intensity and extends the residence time of the fuel–air mixture within the flame stabilization region. As a result, fuel droplets are more effectively entrained into the recirculating flow, improving evaporation and mixing uniformity to approximately 1:23 fuel/air ratio mixture prior to combustion.

Despite the overall new injector configuration generally gives an improvement in fuel/air mixing mechanism , several injectors in the modified configuration (injectors 2, 5, 8, and 9) that is associated with cutting plane angle 65°, 163°, 261°, and 294° still exhibit relatively weak or unstable recirculation zones and has a liner near wall position. This behaviour may be attributed to local imbalances between the annular inlet airflow velocity (U) and the fuel mass flow rate. Nevertheless, the overall flow characteristics of the modified configuration demonstrate a substantial enhancement compared to the original injector arrangement. Fuel distribution was enhanced by the 18.2% drop in mf per injector; however, three injectors (roughly 27% of the total) failed to reach the optimal distribution level because of secondary flow interference. (Topal et al., 2015) found that air speeds above 200 m/s decreased circulation stability.

**Table 3-3:** Data From Numerical Simulation of Injector Modification

| Angle | New Injector Position | Angle | Old Injector Position |
|---|---|---|---|
| 32 |  | 360 |  |
| 65 |  | 40 |  |
| 98 |  | 80 |  |

| Angle | New Injector Position | Angle | Old Injector Position |
|---|---|---|---|
| 130 |  | 120 |  |
| 163 |  | 160 |  |
| 196 |  | 200 |  |
| 229 |  | 240 |  |
| 261 |  | 280 |  |
| 294 |  | 320 |  |
| 327 |  | | |
| 360 |  | | |

An increase in homogeneity is indicated by the density and velocity distribution of the mixture. The velocity shows that the largest injector mixture creates a mixture layer that is consistent with the primary zone and effectively lowers the primary flow. Furthermore, the mixture progressively drops in the middle combustion zone, and the static temperature contours is ranging from 325K to 330K, represent the static temperature values obtained from the numerical simulation of the combustion chamber inlet. Since combustion had not yet taken place in the combustion chamber, these values were recorded.

Flow patterns presented in Table 3-3 show that moving the injectors to the revised location produces a more distinct primary recirculation zone and improves fuel–air interaction within the combustor. As a result, the flow becomes more stable and provides more favorable conditions for flame stabilization. The modified injector arrangement produces more favorable combustion characteristics than the original configuration.

### 3.3 Injector Placement Combustion Simulation Result

The combustion of propane ($C_3H_8$) was evaluated using an inlet temperature of 390.5 K and an inlet pressure of 275,538.43 Pa. The fuel was supplied at stoichiometric conditions ($\Phi$ = 1, FAR = 0.064). The calculated outlet temperature was 1,195.99 K, corresponding to a temperature ratio (TR) of 3.064. The combustion efficiency obtained from the simulation was about 95%. A pressure ratio (PR) of 0.39 was obtained, which corresponds to a pressure loss of 61%. The relatively large pressure loss indicates that the current combustor geometry still needs improvement.

Figures 3-5 to 3-8 show the temperature and pressure fields obtained from the combustion simulation. Both quantities vary along the combustion chamber rather than remaining constant. The data shown for points 3–20 in Figure 3-7 were obtained by averaging the conditions over the liner section illustrated in Figure 3-8. A maximum temperature of 2,239.25 K was found in the primary reaction zone. This region has the most active combustion and therefore experiences the largest temperature increase. Further downstream, the temperature drops after leaving the primary zone. A small increase can then be seen in the secondary zone, where the remaining fuel continues to mix and react with the surrounding air.

Air entering through the dilution-zone ports contributes to the cooling of the combustion products before they leave the combustor. The dilution air lowers the gas temperature in the downstream section and helps limit the thermal load on the liner. Near the injector, the temperature field is also important because the local conditions affect the start of the combustion process. As illustrated in Figure 3-5, areas with temperatures considerably below the ignition temperature of propane may not provide sufficient conditions for flame initiation. In such areas, the fuel may not burn completely.

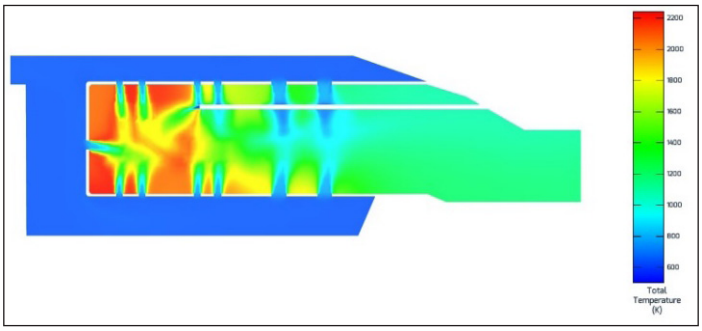



**Figure 3-5:** Total Temperature Distribution During Combustion

Under ideal combustion conditions, the value of TR > 1 due to the release of thermal energy, resulting in $T_{03}T_{03}$ being significantly higher than $T_{02}$. Simulation Results:

- Inlet temperature $T_{02}$: 390,15 K (after compressor)
- Outlet temperature $T_{03}$: 1195.9929 K
- Temperature Ratio (TR): 3.064

The 206.6% increase in temperature (TR = 3.064) indicates intense combustion with substantial chemical energy release and need more air cooling via dilution zone to achieve total temperature target $T_{03}$ = 997.51 K at combustor outlet, achieving temperature ratio to 1:2.55, so that this value aligns with modern gas turbine engines, where TR typically ranges between 2.0–2.5 for stoichiometric mixtures, confirming the simulation's realism.

Value of the PR below unity under normal operating conditionsare expected due to thermal energy conversion during the combustion process.

Simulation data reveals (Figure 3-6):

- Inlet total pressure ($P_{02}$): 281,373.23 Pa (post-compressor stage)
- Outlet total pressure ($P_{03}$): 110,980.2 Pa
- Total pressure ratio difference ($\Delta p_0$): 60%

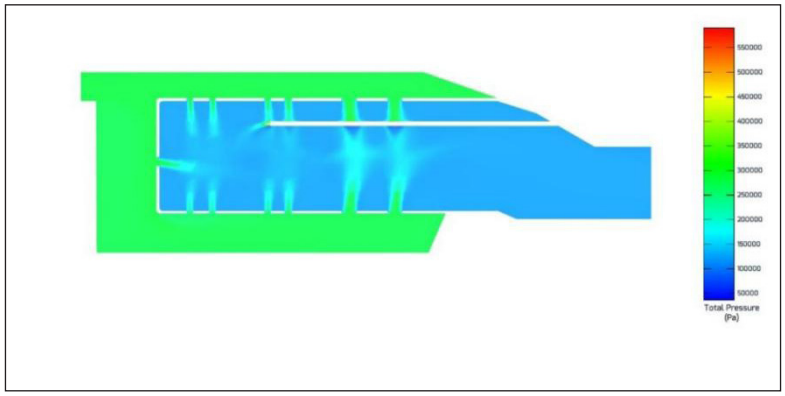



**Figure 3-6:** Total Pressure Distribution During Combustion

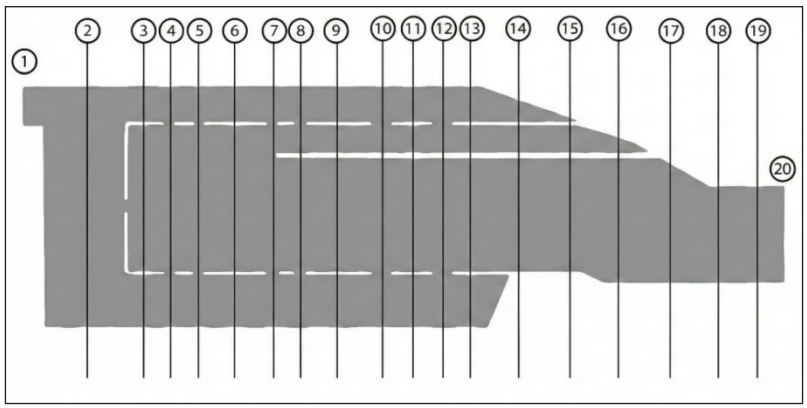



**Figure 3-7:** Combustion Chamber Cross-Sectional Position

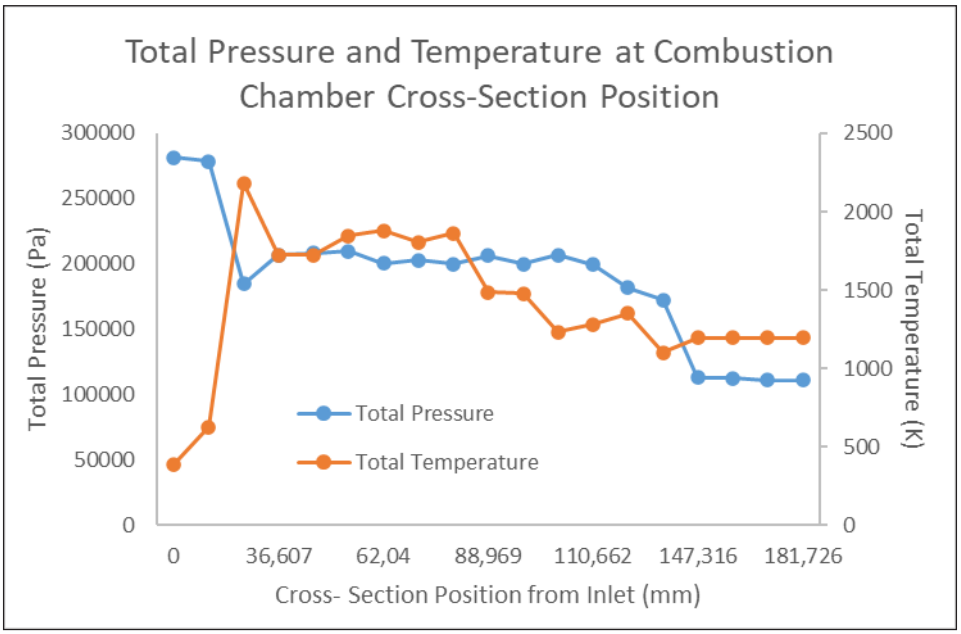



**Figure 3-8:** Mean Total Pressure and Temperature at Combustion Chamber Cross-Section Position

The total pressure value reduces significantly by 30% when the air entering combustion chamber liner. This reducing total pressure caused by the air dynamic pressure content mostly blocked by liner wall and just allowed the air entering liner via liner holes. Furthermore, the total pressure is continued to drop by 30% starting at point 15 where at this point the liner cross section area is reduce to accelerate combustion gas velocity toward to the turbine inlet (expansion process).

CFD analysis reveals a complex velocity profile in the combustion chamber. It has an outlet absolute velocity at 114 m/s that is increasing for 14% compared to design point at 99.79 m/s, and with a high-speed core flow (~200 m/to 300 m/s) surrounded by low-velocity recirculation zones (~60 m/s) at the primary zone region. The velocity difference between the flow streams generates a toroidal vortex that plays an important role in flame stabilization. As shown in Figure 3-9, the rotational flow enhances fuel–air mixing, which contributes to more stable combustion. CFD visualizations show that the toroidal vortex structures are formed by the interaction between the incoming axial flow, the surrounding annular air stream, and the injected fuel jets. These vortices increase the residence time of the fuel–air mixture within the high-temperature region and allow the combustion process to continue for a longer period. As a result, flame stability is improved and combustion efficiency is enhanced.

The airflow distribution consists of 0.112 kg/s in the primary zone, 0.148 kg/s in the secondary zone, and 0.304 kg/s in the dilution zone. The airflow in the primary zone contributes to the formation of the vortex core, while the secondary zone helps maintain flame stability. Air introduced through the dilution zone reduces the temperature of the combustion products without significantly disturbing the vortex structure. This airflow distribution provides favorable conditions for stable and efficient combustion within the mini turbojet combustor.

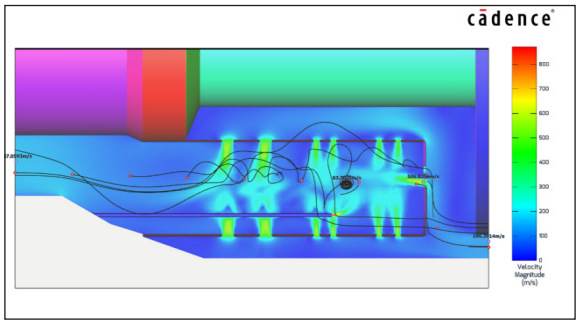



**Figure 3-9** : Formed Recirculation Zone and Air Streamlines During Combustion

At a propane mass flow rate of 0.007425 kg/s and a lower heating value (LHV) of 46,350 kJ/kg, the theoretical heat input was calculated to be 344.1 kW. From the calculated increase in airflow enthalpy across the combustor, an effective thermal output of approximately 298.5 kW was obtained. Accordingly, combustion efficiency was defined as the ratio between the effective thermal output and the theoretical chemical energy input of the fuel, which is consistent with definitions commonly adopted in gas turbine and micro-turbojet combustor performance analyses (Lefebvre & Ballal, 2010; Saravanamuttoo et al., 2017). Based on this definition, the combustion efficiency obtained in the present study was 78.29%.

This efficiency can be classified as relatively high for mini turbojet combustors, as combustion efficiencies reported in similar small-scale and micro-turbine combustion chambers typically range between 65% and 75% (Capata & Achille, 2018; Poinsot & Veynante, 2012). These limitations are mainly attributed to short residence time, high flow velocities, and insufficient primary recirculation strength. Several numerical and experimental studies have indicated that weak recirculation zones and non-uniform fuel–air mixing are the primary factors limiting combustion efficiency in compact combustors (Lefebvre & Ballal, 2010; Fuchs et al., 2019). The new injector arrangement gives a better flow pattern in the primary zone. Placing the injectors closer to the recirculation region increases the interaction between the fuel jet and the surrounding air. The CFD results show that the fuel–air mixture is more evenly distributed in this region, while the recirculation zone is also more developed. These conditions make it easier for the flame to remain in the primary zone. More effective mixing allows the fuel to burn more completely and reduces combustion losses.

## 4. Conclusion

The fuel–air mixing process and combustion behavior were studied using CFD simulations. The flow analysis was first carried out without combustion under steady-state conditions. This allowed the flow inside the combustion chamber to be observed before the combustion calculation was performed. Particular attention was given to the primary recirculation zone and the vortices that developed near the liner wall. The combustion simulation was then carried out under the same steady-state condition. The temperature field, pressure loss, and combustion efficiency were obtained from the results. The fuel–air distribution and the velocity and pressure fields were also examined to compare the flow conditions between the injector configurations.

Changing the injector position changed the flow pattern inside the combustion chamber. The effect was most noticeable around the primary recirculation zone and near the liner wall, where the fuel jet interacted with the surrounding airflow. Variations in these parameters altered the fuel–air mixing process, modified the strength of the recirculation zone, and

influenced the thermal loading experienced by the liner. Based on these findings, the optimized injector configuration improves mixing uniformity indicating by recirculation zone forming on seven out of eleven injector with its center of recirculation zone position and size respectively at x = 4.92 mm, z = 5.52 mm, 10.25 mm in diameter, and performing fuel/air ratio mixture approximately to 1:23 comparing to the previous injector configuration. This improved injector configuration enhances flame stabilization, and reduces undesirable near-wall flow structures. Furthermore, from injector new placement combustion simulation result, the temperature ratio is achieving value at 3.064. This value is higher than targeted design, and indicating more air cooling is needed from dilution zone. The pressure losses at combustion chamber outlet in this combustion simulation is very large at 60%. This high-pressure loss is happened due to combustion chamber design at the outlet where the expansion process resulting a very large total pressure drop and increasing outlet gas velocity (14% in increment) comparing to the outlet gas velocity targeted design at the outlet combustion chamber.

The outcomes of this study are expected to serve as a basis for further investigations, including combustion chamber optimization for reducing pressure loss and outlet velocity by combustion chamber outlet redesign/optimization, reducing temperature ratio by optimizing dilution zone, performing combustion simulations with LES turbulence model or fully unsteady for more accurate prediction and experimental validation, to refine the combustor design and confirm the numerical results under realistic operating conditions.

## 5. Acknowledgements

The author would like to thank Powerplant Laboratory for facilitating the numerical simulation. The author also acknowledges the use of artificial intelligence (AI)-based tools to assist with language editing and proofreading of the manuscript. The authors remain fully responsible for the content, analysis, and conclusions presented in this manuscript.

## 6. Contributorship Statement

ASM developed the simulation and prepared the manuscript; VW served as mentor and supervisor; RFNA obtained the optimized injector position data from the numerical simulation; RSK also served as examiner.

## 7. References

Abubakar, Z., & Mokheimer, E. M. A. (2020). Thermoacoustic combustion instability of propane-oxy-combustion with CO2 dilution: Experimental analysis. *International Journal of Energy Research*, *44*(2), 1031–1045. https://doi.org/10.1002/er.4980

Anggraeni, W. (2022). *Perancangan Injektor Ruang Bakar Mini Turbojet Engine Dengan Thrust Statik 200 N, Laporan Tugas Akhir, Politeknik Negeri Bandung.*

Anissa, R. F. N. (2023). *Analisis Dan Modifikasi Penempatan Injektor Pada Ruang Bakar Mini Turbojet Engine Dengan Gaya Dorong Statik 200 N. Laporan Tugas Akhir, Politeknik Negeri Bandung.*

Capata, R., & Achille, M. (2018). Design and optimization of fuel injection of a 50 kw micro turbogas. *Designs*, *2*(2), 1–22. https://doi.org/10.3390/designs2020014

Chmielewski, M., Fulara, S., & Gieras, M. (2016). Theoretical Studies of Variable Geometry – Hot Section of the Miniature Jet Engine. *Journal of KONES. Powertrain and Transport*, *23*(2), 69–80. https://doi.org/10.5604/12314005.1213559

Elhaj Mohammed, R. S. (2019). Design and Analysis of Annular Combustion Chamber for a Micro Turbojet Engine. *International Journal of Aerospace and Mechanical Engineering, International Scholarly and Scientific Research & Innovation*, *13*(4), 282–287.

Fuchs, F., Meidinger, V., Neuburger, N., Reiter, T., Zündel, M., & Hupfer, A. (2019). Challenges in designing very small jet engines - fuel distribution and atomization. *Open Archives of the 16th International Symposium on Transport Phenomena and Dynamics of Rotating Machinery, ISROMAC 2016*, 1–8.

Gieras, M., & Stankowski, T. (2012). Computational study of an aerodynamic flow through a micro-turbine engine combustor. *Journal of Power and Technologies*, *92*(2), 68–79.

Gorgulu, Y. F., Sahin, B., Ekici, S., & Karakoc, T. H. (2025). Altitude-Dependent Analysis of Combustion Performance and Emissions in a Commercial Aircraft Engine Leveraging Real Engine Data. *International Journal of Aeronautical and Space Sciences*, *June*. https://doi.org/10.1007/s42405-025-00982-y

H.I.H. Saravanamuttoo, H. Cohen, G. F. C. R., & A.C. Nix, P. V. S. (2017). *Gas Turbine Theory SEVENTH EDITION Gas Turbine Theory*.

He, W., Guo, Z., Xu, S., & Jin, Y. (2021). Numerical and Experimental Investigations on Performance Optimization of a Microturbojet Engine Combustor. *International Journal of Aerospace Engineering*, *2021*. https://doi.org/10.1155/2021/6616537

PRISACARIU, V., & CÎRCIU, I. (2016). Considerations Regarding the Performance of Combustion Chambers for Turbo-Jet Engines. *Review of the Air Force Academy*, *14*(2), 53–60. https://doi.org/10.19062/1842-9238.2016.14.2.7

Santoso, R. R., Wuwung, V., Fadjrin, R., Annisa, N., & Kartanegara, R. S. (2023). Design of Mini Turbojet Engine Combustion Chamber Liner With 200N Static Thrust. *Santoso et Al.) Indonesian Journal of Aerospace*, *21*(2), 65–82. https://doi.org/10.55981/ijoa.2023.38

Syarifudin, A., & Bramantya, M. A. (2022). Simulasi Numerik Pengaruh Jumlah Fuel Injector dan Dimensi Lubang Liner Ruang Bakar Turbojet 200 N. *Journal of Mechanical Design and Testing*, *4*(1), 32. https://doi.org/10.22146/jmdt.63201

Topal, A., Turan, O., & Uslu, S. (2015). Design, Manufacturing and Rig Test of a Small Turbojet Engine Combustor with Airblast Atomizer. *International Journal of Materials, Mechanics and Manufacturing*, *3*(2), 97–100. https://doi.org/10.7763/ijmmm.2015.v3.174

Wu, Y., Al-Rahbi, I. S., Lu, Y., & Kalghatgi, G. T. (2007). The stability of turbulent hydrogen jet flames with carbon dioxide and propane addition. *Fuel*, *86*(12–13), 1840–1848. https://doi.org/10.1016/j.fuel.2006.11.032

Zhang, Z., Zhao, D., Ni, S., Sun, Y., Wang, B., Chen, Y., Li, G., & Li, S. (2019). Experimental characterizing combustion emissions and thermodynamic properties of a thermoacoustic swirl combustor. *Applied Energy*, *235*(October 2018), 463–472. https://doi.org/10.1016/j.apenergy.2018.10.130

Z. P. Tan. (2017) “Experimental Study of Spray-Formation Processes in Twin-FluidJet-In-Cross-flow At Jet-Engine Operating Conditions”, Ph.D Thesis, Georgia Institute of Technology.